Noncanonical function of DGCR8 controls mESC exit from pluripotency

Daniel Cirera-Salinas,[1] Jian Yu,[1,2] Maxime Bodak,[1,2] Richard P. Ngondo,[1] Kristina M. Herbert,[3] and Constance Ciaudo[1]

[1]Department of Biology, Institute of Molecular Health Sciences, RNAi and Genome Integrity, Swiss Federal Institute of Technology Zurich, Zurich 8093, Switzerland
[2]Life Science Zurich Graduate School, University of Zurich, Zurich 8093, Switzerland
[3]Sanford Burnham Prebys Medical Discovery Institute, La Jolla, San Diego, CA 92037

Mouse embryonic stem cells (mESCs) deficient for DGCR8, a key component of the microprocessor complex, present strong differentiation defects. However, the exact reasons impairing their commitment remain elusive. The analysis of newly generated mutant mESCs revealed that DGCR8 is essential for the exit from the pluripotency state. To dissociate canonical versus noncanonical functions of DGCR8, we complemented the mutant mESCs with a phosphomutant DGCR8, which restored microRNA levels but did not rescue the exit from pluripotency defect. Integration of omics data and RNA immunoprecipitation experiments established DGCR8 as a direct interactor of Tcf7l1 mRNA, a core component of the pluripotency network. Finally, we found that DGCR8 facilitated the splicing of Tcf7l1, an event necessary for the differentiation of mESCs. Our data reveal a new noncanonical function of DGCR8 in the modulation of the alternative splicing of Tcf7l1 mRNA in addition to its established function in microRNA biogenesis.

Introduction

The canonical miRNA pathway has an important role in stem cell biology, regulating features such as pluripotency and cell fate commitment, and its misregulation contributes to human diseases. miRNAs are processed from primary transcripts in the nucleus by the microprocessor complex, which consists of the RNase III enzyme DROSHA and two DGCR8 double-stranded RNA-binding proteins to generate precursor miRNAs (Nguyen et al., 2015; Herbert et al., 2016). Precursor miRNAs are then exported into the cytoplasm and processed by DICER to generate mature miRNAs. They are then incorporated into the RNA-induced silencing complex, leading to the destabilization or translational repression of their target transcripts (Ambros, 2003; Bartel, 2009).

Several proteins involved in miRNA biogenesis are regulated by posttranslational modifications (Kim et al., 2009). In particular, the ability of DGCR8 to bind RNA is modulated by dimerization, in concert with acetylation and phosphorylation (Wada et al., 2012; Herbert et al., 2013). The phosphorylation of DGCR8 conditions its ability to associate with cofactors. Although DGCR8 phosphorylation increased its stability, it did not alter its miRNA processing activity, suggesting novel functions for this posttranslational modification (Herbert et al., 2013). Importantly, noncanonical functions for DGCR8 have been recently discovered, including the binding to a large number of structured RNAs that harbor predicted secondary structures resembling that of a primary miRNA, and to cassette exons regulating the abundance of alternative spliced isoforms (Macias et al., 2012). Finally, recent work revealed an interplay between pre-mRNA splicing and the microprocessor within the supraspliceosome (Agranat-Tamir et al., 2014).

DGCR8's function is essential for mouse embryonic development, reflected by embryonic lethality postimplantation (Wang et al., 2007). Interestingly, *Dgcr8* knockout (*Dgcr8*_KO) mouse embryonic stem cells (mESCs) present proliferation and differentiation defects that slightly differ from those of *Dicer* mutant mESCs (Kanellopoulou et al., 2005; Wang et al., 2007), suggesting miRNA-independent functions in the differentiation process. Several transcription factors are critical for the maintenance of the naive pluripotent state of mESCs, including OCT4, SOX2, and NANOG (OSN). Their down-regulation is essential to exit pluripotency and differentiate in the three germ layers (Loh et al., 2015). TCF7L1 (also known as TCF3) is an integral component of the core pluripotency network and shares many DNA-binding sites with OSN (Tam et al., 2008). Its down-regulation or disruption leads to an enhancement of the self-renewal capacity of mESCs and a resistance to differentiation (Yi et al., 2008; Guo et al., 2011). Furthermore, Tcf7l1 mRNA is present as two alternatively spliced isoforms in mESCs. The Tcf7l1 isoforms have similar transcriptional activities in the regulation of mESC renewal

Correspondence to Constance Ciaudo: cciaudo@ethz.ch

Abbreviations used: DGCR, DiGeorge syndrome critical region; EB, embryoid body; LIF, leukemia inhibitor factor; mESC, mouse embryonic stem cell; RIP, RNA immunoprecipitation; RNA-seq, RNA sequencing; sgRNA, single guide RNA; WT, wild type.

The Rockefeller University Press $30.00
J. Cell Biol. Vol. 216 No. 2 355–366
https://doi.org/10.1083/jcb.201606073

and distinct activities in the regulation of their differentiation (Salomonis et al., 2010).

Here, we discovered a new role for the DGCR8 protein, independent of DROSHA, regulating the exit from pluripotency of mESCs. Moreover, the impaired differentiation of *Dgcr8*_KO mESCs is independent of its function in miRNA biogenesis. Importantly, proper phosphorylation of the protein is required for DGCR8 binding to Tcf7l1 pre-mRNA to facilitate pre-mRNA splicing to the short isoform and thereby control the exit from pluripotency of mESCs. Together, these data reveal a new noncanonical function for DGCR8 protein as a key regulator of the core pluripotency network in mESCs.

Results and discussion

*Dgcr8*_KO mESCs do not exit the pluripotency state

The fact that *Dgcr8* and *Dicer* mutant mESCs have distinct phenotypes indicates that putative noncanonical functions of DGCR8 or the role of DICER in the siRNA pathway could be the underlying cause of these differences (Kanellopoulou et al., 2005; Wang et al., 2007). To understand the molecular mechanisms causing the differentiation defects in *Dgcr8* mutant mESCs (Wang et al., 2007), we generated new CRISPR/Cas9 mutant cells for the *Dgcr8* gene, which mimic the deletion of previously described $Dgcr8^{\text{Cre-lox}}$ mutant mESCs (Wang et al., 2007). Two independent genomic deletion events were achieved using CRISPR/Cas9 single guide RNAs (sgRNAs) targeting the nuclear localization domain of DGCR8 (Fig. 1 A). Independent mESC clones were isolated and the deletion of *Dgcr8* confirmed at the DNA and protein levels (Fig. S1A and Fig. 1 A), leading to a strongly reduced expression of canonical precursor (Fig. S1 B) and mature miRNAs (Fig. S1, C and D). Conversely, expression of miR-320 (a microprocessor-independent miRNA) was not substantially affected (Fig. S1 C). These mutant cells proliferated at a significantly slower rate than their wild-type (WT) counterparts and presented a G1 phase arrest (Fig. S1, E and F).

To assess the differentiation capacity of these mutant mESCs, we performed an embryoid body differentiation (EB) assay (Fig. 1 B). Molecular analysis revealed that *Dgcr8*_KO mESCs failed to repress the core pluripotency network and to induce the expression of differentiation markers from the three germ layers (Fig. 1, B and C; and Fig. S1 G). Collectively, newly generated *Dgcr8*_KO mESCs are impaired in their differentiation capacity.

To investigate the commitment to differentiation of our knockout mESCs, we performed an exit from pluripotency assay (Fig. 1 D; Betschinger et al., 2013). Both *Dgcr8*_KO clones were positive for AP staining and presented stem cell morphology, whereas WT mESCs died or were AP negative (Fig. 1 D). These results indicate that DGCR8 is essential for the exit from pluripotency of mESCs. Furthermore, FACS analysis of the coexpression of OCT4/NANOG and STELLA/SSEA-1 pluripotent markers revealed that *Dgcr8*_KO mESCs cultured in serum plus leukemia inhibitor factor (LIF) conditions presented a reinforced pluripotency network compared with WT mESCs (Fig. 1 E and Fig. S1, H and I), similar to cells grown in 2i medium (not depicted; Marks et al., 2012). These experiments show that the regulatory circuitry of pluripotent cells can be sustained without DGCR8, but it is necessary to exit from the self-renewal program and initiate differentiation.

Phosphomutant-complemented *Dgcr8*_KO mESCs rescue miRNA phenotypes but cannot exit the pluripotent state

23 phosphorylation sites have been mapped on the DGCR8 protein (Herbert et al., 2013). Mutation of all of these sites has been shown to have no impact on miRNA biogenesis. Nevertheless, their role in noncanonical functions of DGCR8 has not been assessed yet. To rescue phenotypes observed in the *Dgcr8*_KO mESCs, we complemented our *Dgcr8*_KO mESCs with WT mouse (mouse), WT human (human), and a phosphomutant (mutant) human DGCR8 (described in Herbert et al., 2013). DGCR8 protein levels were recovered in all complemented clones (Fig. 2 A), and the presence of the deletion in the endogenous *Dgcr8* locus was also confirmed (Fig. S2 A). It has previously been shown that the absence of miRNA destabilizes Argonaute 2 (AGO2) protein, an important member of the RNA-induced silencing complex (Smibert et al., 2013). Indeed, miRNAs and AGO2 protein levels were strongly reduced in *Dgcr8*_KO mESCs and restabilized in the complemented clones (Figs. 2 A and S2 B). Moreover, the expression of known miRNA target genes was also restored, validating the functionality of the miRNAs (Fig. 2 B). Likewise, previous studies demonstrating the role of miRNAs regulating proliferation and the cell cycle (Cirera-Salinas et al., 2012; Wang et al., 2013), distribution profiles, and proliferation rates were fully restored in all complemented clones (Fig. S2, C and D). Collectively, the complementation of *Dgcr8*_KO mESCs with the different forms of DGCR8 recovered miRNA production, the proliferation defect, and cell cycle distribution. Of note, the 23 phosphorylation sites of DGCR8 protein do not map to the DROSHA-binding site (Herbert et al., 2013). Therefore, it is not surprising that the function of DGCR8 in the biogenesis of miRNAs is not altered in the complemented mESCs.

Surprisingly, the phosphomutant ($Dgcr8^{mutant}$) DGCR8-complemented mESCs were not able to differentiate, similar to *Dgcr8*_KO mESCs (Fig. 2 C and Fig. S2, E and F). Indeed, FACS analysis of the OSN proteins after 10 d of differentiation indicated that *Dgcr8*_KO and $Dgcr8^{mutant}$ mESCs still expressed these proteins. In contrast, fewer WT or DGCR8-complemented (mouse and human) cells were positive for these factors (Fig. S2, E and F). Additionally, *Dgcr8*_KO and $Dgcr8^{mutant}$ failed to differentiate to a directed neuronal precursor cell differentiation (unpublished data). These results reveal that correct posttranslational modifications of DGCR8 protein are essential for the early differentiation process.

Finally, an exit from pluripotency assay demonstrated that similar to *Dgcr8*_KO, $Dgcr8^{mutant}$ were not capable of exiting from the pluripotency state (Fig. 2 D). Collectively, these results indicate that $Dgcr8^{mutant}$ mESCs are not able to exit pluripotency, despite a restoration of miRNAs expression, cell proliferation, and proper cell cycle distribution. Therefore, we hypothesized that the exit from pluripotency impairment observed in *Dgcr8*_KO mESCs might be independent of the role of DGCR8 in the miRNA biogenesis pathway. Furthermore, the phosphorylation of DGCR8 could represent another mechanism ensuring tight control of the exit from pluripotency in mESCs.

DGCR8 binds Tcf7l1 mRNA, a component of the core pluripotency network

To understand the underlying molecular mechanisms responsible for the block of pluripotency exit in *Dgcr8*_KO mESCs, we first assessed the transcriptome of WT and *Dgcr8*_KO

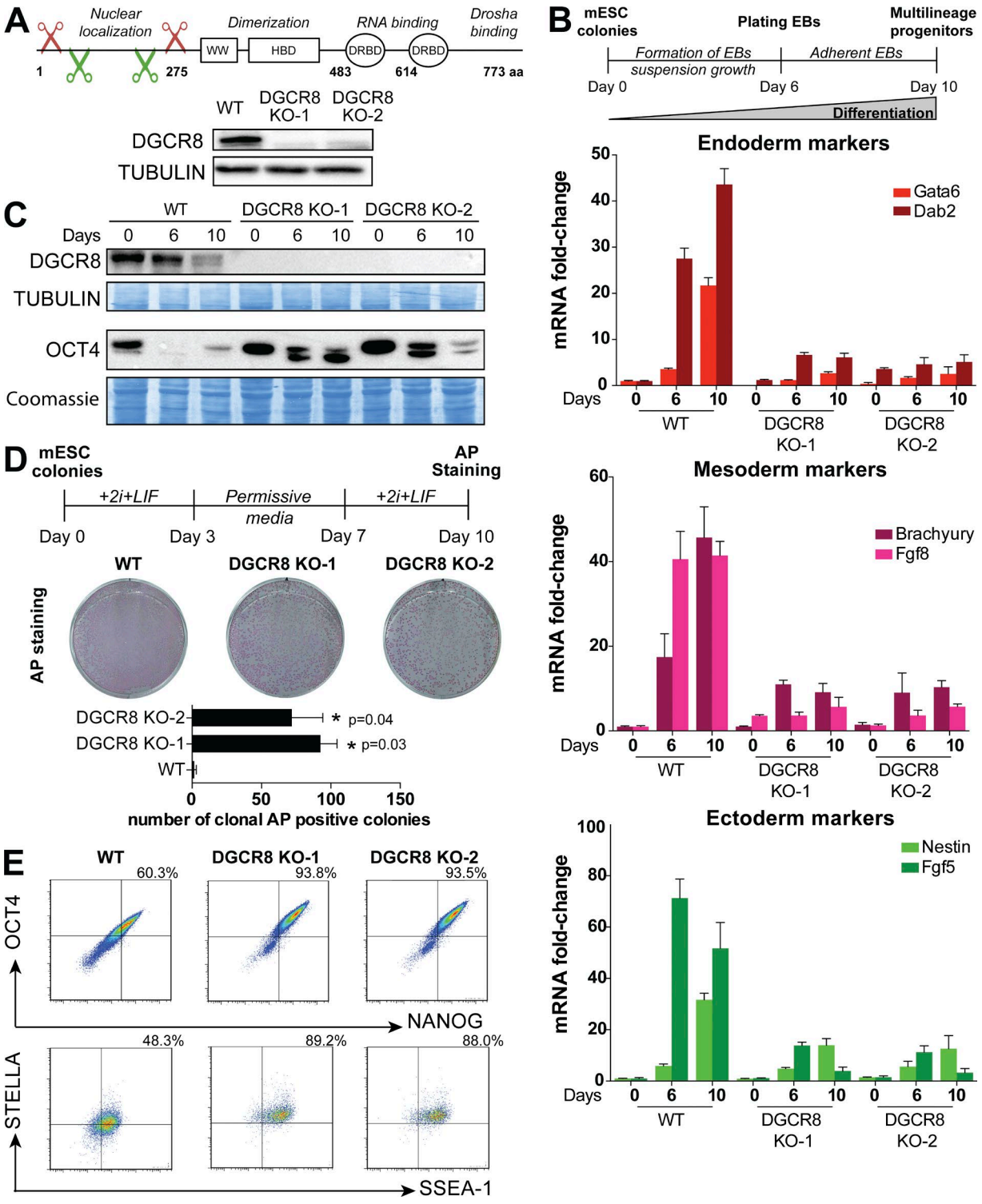

Figure 1. **Differentiation and commitment defects of CRISPR-Cas9–generated *Dgcr8*_KO mESCs.** (A) *Dgcr8* mouse gene CRISPR-Cas9 schematic design. WW corresponds to the Rsp5 domain of the DGCR8 protein, HBD stands for histone binding domain, and DRBD stands for double-stranded RNA binding domain. Immunoblot analysis of DGCR8 in WT and *Dgcr8*_KO mESCs. (B) Illustration of the embryoid body (EB) differentiation assay. Quantitative RT-PCR analysis of the differentiation markers (endoderm: Gata6 and Dab2; mesoderm: Brachyury and Fgf8; ectoderm: Nestin and Fgf5) in WT and *Dgcr8*_KO mESCs during EB differentiation. The data are shown as the fold change compared with WT cells at day 0 after normalization to the *Rrm2* housekeeping gene. Error bars are the mean ± SEM and are representative of three or more experiments. (C) Immunoblot analysis of DGCR8 and the pluripotent marker OCT4 after EB differentiation in WT and *Dgcr8*_KO mESCs. Membranes were stained with Coomassie to ensure equal loading. (D) Schematic representation of exit from pluripotency assay. Clonal AP staining of cells after exit from pluripotency assay. AP staining was performed in triplicate, and a representative example is shown. Error bars are the mean ± SEM and are representative of three independent experiments. *, $P < 0.05$; Student's *t* test. (E) Flow cytometry analysis of OCT4/NANOG and STELLA/SSEA-1 in WT and *Dgcr8*_KO mESCs. Representative plots of three or more experiments are shown.

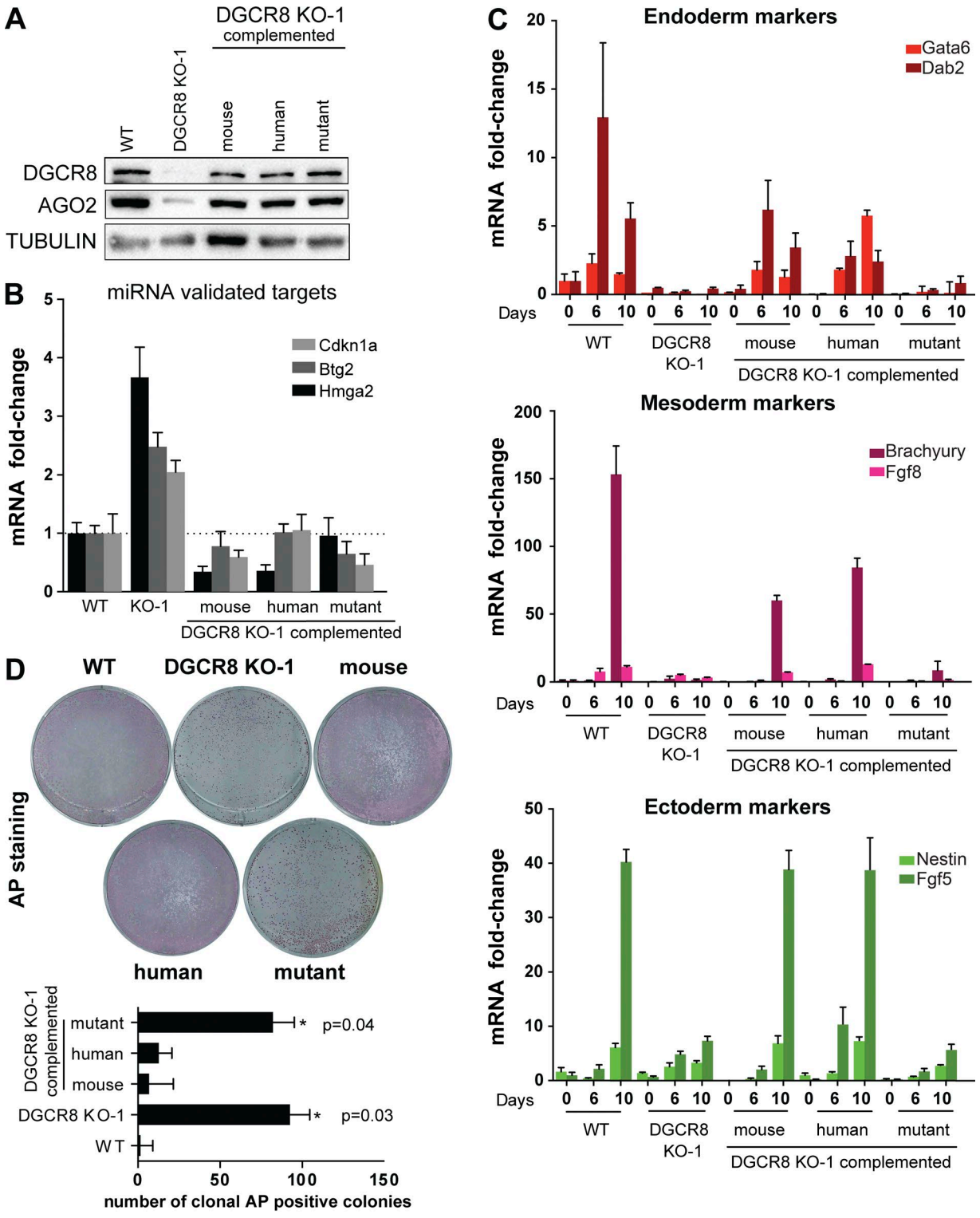

Figure 2. **Phosphomutant DGCR8 complementation of *Dgcr8*_KO mESCs rescues miRNA biogenesis, but not the differentiation or impaired pluripotency exit.** (A) Immunoblot analysis of DGCR8 and AGO2 proteins in WT, *Dgcr8*_KO, and complemented *Dgcr8*_KO mESCs. Expression of α-tubulin was used as a loading control. (B) Quantitative RT-PCR analysis of validated miRNA target genes in WT, *Dgcr8*_KO, $Dgcr8^{mouse}$, $Dgcr8^{human}$, and $Dgcr8^{mutant}$ mESCs. The data are shown as the fold change compared with WT cells at day 0 after normalization to the *Rrm2* housekeeping gene. Error bars are the mean ± SEM and are representative of three independent experiments. (C) Quantitative RT-PCR analysis of differentiation markers (endoderm: Gata6 and Dab2; mesoderm: Brachyury and Fgf8; ectoderm: Nestin and Fgf5) in WT and *Dgcr8*_KO and complemented *Dgcr8*_KO mESCs. The data are shown as the fold change compared with WT cells at day 0 after normalization to the *Rrm2* housekeeping gene. Error bars are the mean ± SEM and are representative of three independent experiments. (D) Clonal AP staining after exit from pluripotency assay in WT, *Dgcr8*_KO, and complemented *Dgcr8*_KO mESCs. Error bars are the mean ± SEM and are representative of three or more experiments. *, $P < 0.05$; Student's *t* test.

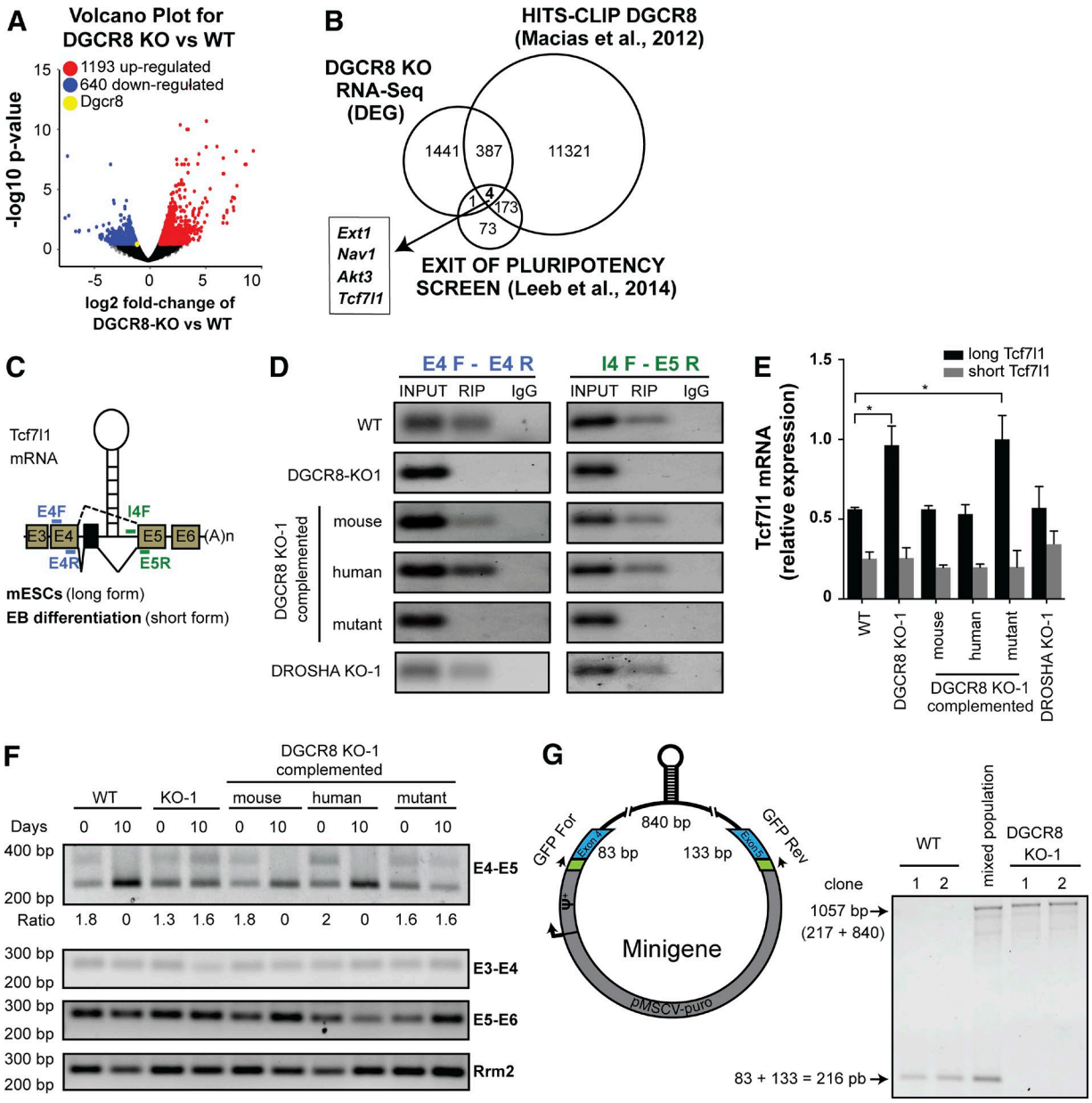

Figure 3. **DGCR8 directly interacts with Tcf7l1 in a RNA-dependent manner and facilitates its alternative splicing.** (A) Volcano plot showing the global transcriptional changes in *Dgcr8*_KO versus WT mESCs. The x axis shows the log fold change, and the y axis shows the −log10 of the p-value. Differentially expressed genes are represented by colored circles and are defined by a fold change greater than two and a false discovery rate <0.1. (B) Venn diagram showing the intersection between our RNA-seq, a DGCR8 HITS-CLIP (Macias et al., 2012), and a candidate list of exit from pluripotency genes (Leeb et al., 2014). (C) Exon structure graph for *Tcf7l1* gene with differences in isoform expression between mESCs and EBs. The detected alternative exon is indicated as a black filled box. Dashed line between exons indicates an alternative splicing event. The hairpin structure in intron 4 is depicted as well. (D) DGCR8-immunoprecipitated RNA from WT, *Dgcr8*_KO, *Drosha*_KO, and complemented *Dgcr8*_KO mESCs. RIP was performed in triplicate, and a representative example is shown. INPUT, RNA isolated from input samples; RIP, RNA isolated from the immunoprecipitated DGCR8; IgG, RNA isolated from the immunoprecipitated IgG control. (E) Quantitative RT-PCR of long and short Tcf7l1 mRNA in WT, *Dgcr8*_KO, complemented *Dgcr8*_KO, and *Drosha*_KO mESCs. The data are shown as relative expression after normalization to the *Rrm2* housekeeping gene. Error bars are the mean ± SEM and are representative of three or more experiments. (F) RT-PCR of alternative splicing events in Tcf7l1 before (day 0) and after 10 d of differentiation (day 10). PCR amplicons from exons 3–4, exons 5–6, and *Rrm2* were used as a control. Ratio: long Tcf7l1/short Tcf7l1. (G) Minigene splicing reporter analysis. Alternative splicing events in 1% agarose gel from independent single clones in WT and *Dgcr8*_KO mESCs. A mixed population of WT cells was used as a control. Representative gels of three or more experiments are shown. *, $P < 0.05$; Student's *t* test.

mESCs by RNA sequencing (RNA-seq). We identified many differentially expressed genes implicated in several biological pathways (Fig. 3 A, Fig. S3 A, and Table S3). The intersection of our RNA-seq data with a DGCR8 HITS-CLIP dataset (mRNA bound by DGCR8; Macias et al., 2012) and a list of candidate genes involved in the exit from pluripotency (Leeb et al., 2014) highlighted only four potential candidates that might be responsible for the observed phenotype: *Ext1*, *Nav1*, *Akt3*, and *Tcf7l1* genes (Fig. 3 B).

We decided to confirm the direct binding of DGCR8 to the stem-loop structure present in intron four of Tcf7l1 mRNA because of its well-established role in the core pluripotency

network (Pereira et al., 2006; Cole et al., 2008; Marson et al., 2008; Tam et al., 2008; Salomonis et al., 2010; Leeb et al., 2014; Fig. 3 C). RNA immunoprecipitation (RIP) experiments demonstrated that DGCR8^{mutant} protein was not able to bind Tcf7l1 mRNA, contrary to WT, DGCR8^{mouse}, and DGCR8^{human} (Fig. 3, C and D; and Fig. S3, B and C). The phosphosite mutations might affect the charge of the protein and therefore change its affinity to Tcf7l1 mRNA. Furthermore, we generated *Drosha*_KO mESCs (Fig. S3 D) and assessed the binding of DGCR8 to Tcf7l1 mRNA. RIP of Tcf7l1 mRNA with DGCR8 protein in *Drosha*_KO mESCs demonstrated that DGCR8 binds Tcf7l1 mRNA independently of the microprocessor complex. These experiments confirm previous studies of interactions between DGCR8 protein and Tcf7l1 mRNA (Macias et al., 2012) and reveal that this interaction is dependent on correct post-translational modifications of DGCR8 protein.

Moreover, we monitored the expression of the four candidates in all mESC clones (Figs. 3 E and S3 E). Only the expression of the long Tcf7l1 isoform was up-regulated in *Dgcr8*_KO and *Dgcr8*^{mutant} clones compared with the other mESCs (Fig. 3 E). Interestingly, the short Tcf7l1 isoform was expressed at comparable low levels among all clones, as expected in undifferentiated stem cells (Salomonis et al., 2010). In conclusion, the ratio between the long and short Tcf7l1 mRNAs was higher in *Dgcr8*_KO and *Dgcr8*^{mutant} clones. Therefore, we hypothesized that the differential expression of the long Tcf7l1 isoform expression could explain the impaired pluripotency exit phenotype observed. Of note, Tcf7l1 was also present in our list of differentially spliced genes in *Dgcr8*_KO mESCs (Table S4).

Subsequently, we demonstrated that after 10 d of differentiation, the two Tcf7l1 isoforms were still detected in *Dgcr8*_KO and *Dgcr8*^{mutant} clones as in undifferentiated mESCs (Fig. 3 F). Furthermore, to assess the role of DGCR8 in the splicing of Tcf7l1 mRNA, we designed a minigene vector harboring, from the *Tcf7l1* gene, exon 4, the part of the intronic region containing the DGCR8 interacting loop, and exon 5 (Fig. 3 G). After transient transfection in WT cells (mixed population), spliced and unspliced isoforms could be detected. Nevertheless, independent stable *Dgcr8*_KO clones were unable to splice the minigene construct, whereas independent stable WT mESCs spliced it correctly (Fig. 3 G). Collectively, these data demonstrate that DGCR8 is essential for the correct splicing of Tcf7l1 mRNA.

DGCR8 controls cell pluripotency and differentiation through the alternative splicing of Tcf7l1 mRNA

Next, we investigated the role of the long Tcf7l1 isoform in the impaired exit from pluripotency phenotype. Down-regulation of the long Tcf7l1 mRNA by siRNA during the exit from pluripotency assay allowed significantly more *Dgcr8*_KO and *Dgcr8*^{mutant} mESCs to commit to differentiation (Fig. 4 A and Fig. S3, F and G). These results suggest a role for the long Tcf7l1 isoform or for an appropriate ratio between the two isoforms in the reinforcement of the pluripotency state in *Dgcr8*_KO and *Dgcr8*^{mutant} mESCs. We detected homogenous coexpression of OCT4/NANOG and STELLA/SSEA-1 pluripotency factors in *Dgcr8*^{mutant} mESCs, similar to *Dgcr8*_KO, contrary to the intermediate heterogeneity observed in WT, *Dgcr8*^{mouse}, and *Dgcr8*^{human} mESCs (Fig. 4 B).

siRNA against the long or short Tcf7l1 isoforms had the most profound overall effect when transfected during differentiation of the cells. *Dgcr8*_KO and *Dgcr8*^{mutant} cell differentiation was partially restored when the long Tcf7l1 was suppressed as shown by the down-regulation of pluripotent markers and the up-regulation of several differentiation makers (Fig. 4 C). Conversely, down-regulation of the short Tcf7l1 isoform inhibited the differentiation of WT mESCs (Fig. 4 C). Moreover, down-regulation of long or short Tcf7l1 isoforms in mESCs had different transcriptomic consequences on known targets (Salomonis et al., 2010), demonstrating the different transcriptional effects of the two isoforms (Fig. S3 H).

To finally demonstrate the importance of the short Tcf7l1 isoform in mESC differentiation, we stably expressed it, in an inducible manner, in WT and *Dgcr8*_KO mESCs. The forced expression of the short Tcf7l1 (Fig. S3 I) caused a dramatic down-regulation of pluripotency (OCT4/NANOG and *Rex1*) and up-regulation of differentiation (*Dnmt3b*) markers in WT and *Dgcr8*_KO mESCs (Fig. 5, A and B). Collectively, these data demonstrate that the down-regulation of the long Tcf7l1 isoform and the up-regulation of the short Tcf7l1 isoform promote the exit from pluripotency and differentiation of mESCs.

In conclusion, DGCR8 is required for the splicing of the long Tcf7l1 isoform and a correct balance between the two isoforms, facilitating the activation of cell lineage–specific programs. We propose a working model recapitulating our findings (Fig. 5 C). Finally, our results explain the previously observed impaired differentiation process of *Dgcr8*_KO mESCs and reveal a new noncanonical function of DGCR8 essential for the exit from pluripotency of mESCs.

Materials and methods

Materials

Chemicals were obtained from Sigma-Aldrich unless otherwise noted.

Cell culture

The E14TG2a mESC (CRL-1821; ATCC) line was used for WT mESCs. Cells were cultured into DMEM (Invitrogen) supplemented with 15% of a selected batch of FBS (Gibco) tested for optimal mESC growth, 1,000 U/ml LIF (EMD Millipore), 0.1 mM 2-β-mercaptoethanol (Thermo Fisher Scientific), 0.05 mg/ml streptomycin, and 50 U/ml penicillin (Sigma-Aldrich). Cells were grown on 0.2% gelatin-coated cell culture–grade plastic vessels in the absence of feeder cells. For the differentiation assays, cells were cultured in differentiation medium composed of DMEM supplemented with 10% FBS, 0.1 mM β-mercapto-ethanol (Thermo Fisher Scientific), 0.05 mg/ml streptomycin, and 50 U/ml penicillin (Sigma-Aldrich). Cells were cultured in suspension in low-adherent tissue culture dishes from day 1 to day 6 and then reattached on adherent 0.2% gelatin-coated flask and collected at day 10. All cells were grown at 37°C in 8% CO_2, and the culture medium was changed daily.

Generation of *Dgcr8*_KO and *Drosha*_KO mESCs using CRISPR/Cas9

*Dgcr8*_KO and *Drosha*_KO mESCs were generated from E14TG2a mESCs using a paired CRISPR/Cas9 strategy (Wettstein et al., 2016). The plasmid pX330-U6-Chimeric_BB-CBh-hSpCas9 (plasmid 42230; Addgene) was used. Cells were single-cell sorted 48 h after transfection using a flow cytometry cell sorter (MoFlo; BD) into 96-well plates (one single cell per well). The first screening for selection of candidates was performed at the genomic level by PCR. All of the primers used for CRISPR/Cas9 constructions and PCR screening are described in Table S1. Specific CRISPR/Cas9 sgRNAs were generated using E-CRISPR software (Heigwer et al., 2014) or alternatively chosen

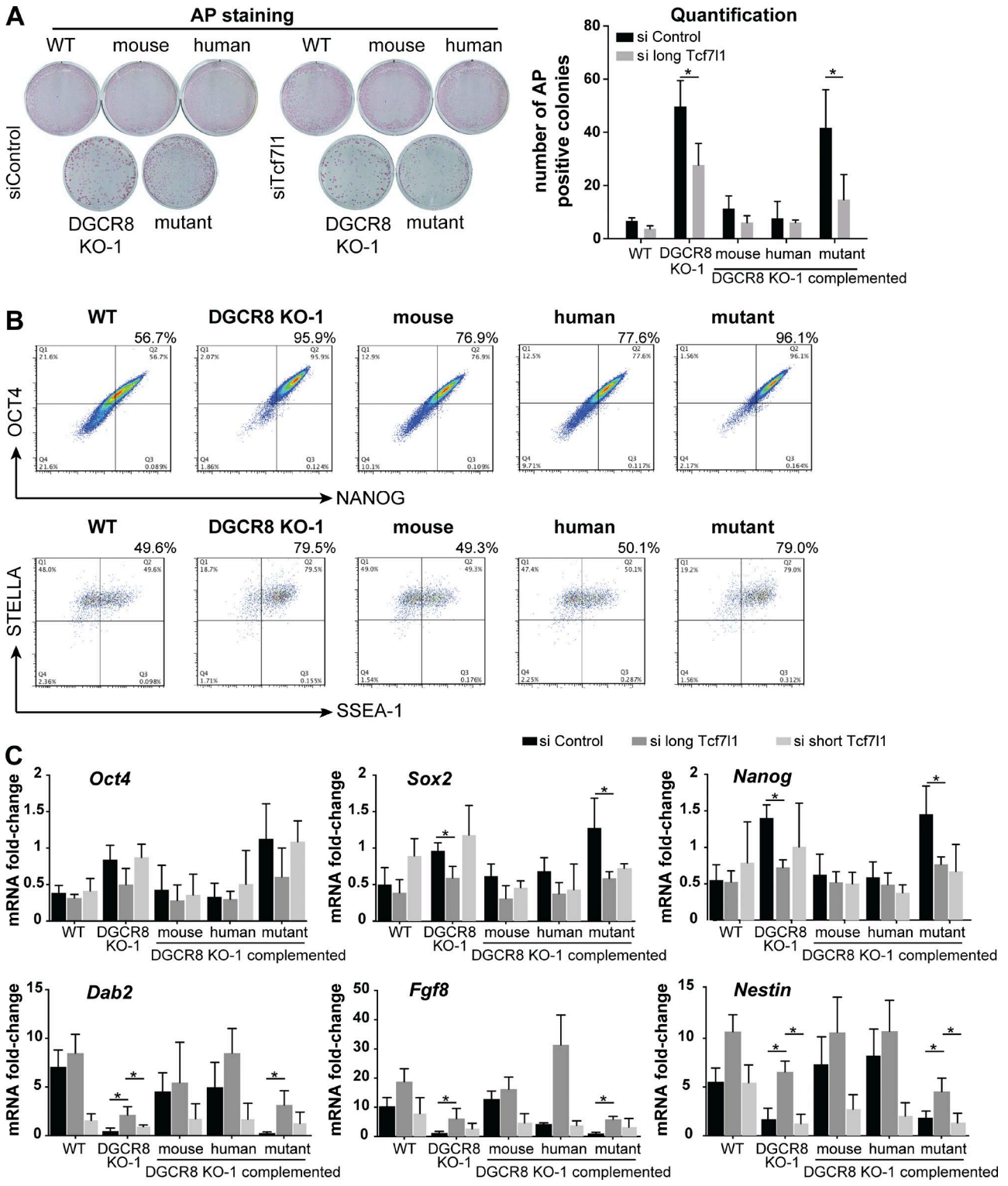

Figure 4. **Down-regulation of long Tcf7l1 promotes exit from pluripotency and differentiation of mESCs.** (A) Exit from pluripotency assay after knockdown of the long Tcf7l1 isoform in WT, *Dgcr8*_KO, and complemented *Dgcr8*_KO mESCs. (B) Flow cytometry analysis of OCT4/NANOG and STELLA/SSEA-1 in WT, *Dgcr8*_KO, and complemented mESCs. Representative plots of three independent experiments are shown. Error bars are the mean ± SEM and are representative of three independent experiments. (C) Quantitative RT-PCR analysis of pluripotency (OSN, top) and differentiation (bottom) markers in WT, *Dgcr8*_KO, and complemented *Dgcr8*_KO mESCs upon knockdown of long or short Tcf7l1 isoforms with siRNA every 48 h. *Rrm2* housekeeping gene was used as reference. For each gene, data were normalized to the mRNA at day 0. Error bars are the mean ± SEM and are representative of three or more experiments. *, $P < 0.05$; Student's *t* test.

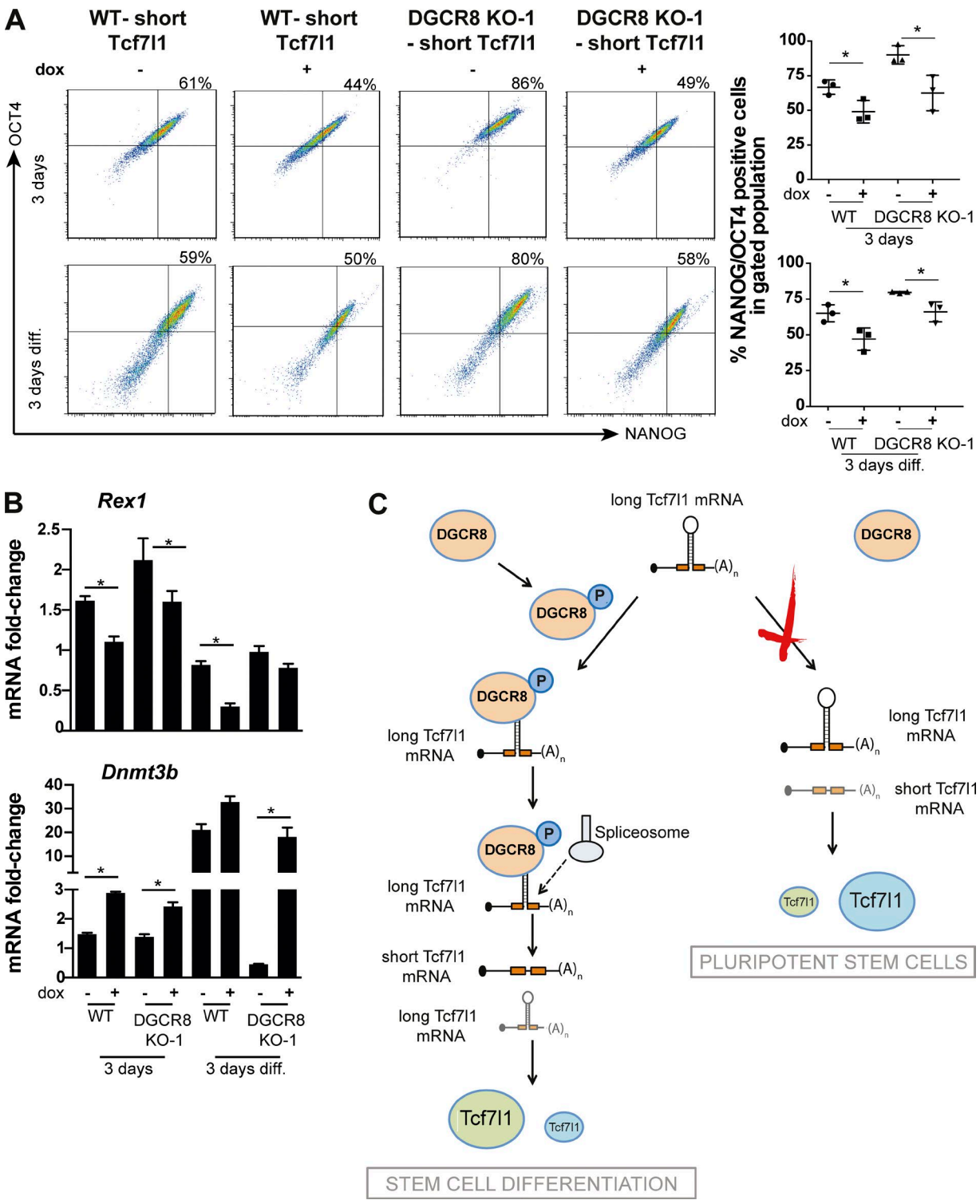

Figure 5. **Up-regulation of short Tcf7l1 promotes exit from pluripotency and differentiation of mESCs.** Flow cytometry analysis of OCT4/ NANOG (A) and quantitative RT-PCR analysis of pluripotent (*Rex1*) or early differentiation (*Dnmt3b*) markers in WT and *Dgcr8*_KO mESCs upon induction of the short Tcf7l1 (+dox) for 3 d in serum plus LIF (top) or differentiation (bottom) media (B). Representative plots of three or more experiments are shown. Quantification is shown on the right. *, $P < 0.05$; Student's *t* test. The data are shown as the fold-change compared with WT cells at day 0 after normalization to the *Rrm2* housekeeping gene. Error bars are the mean ± SEM and are representative of three independent experiments. (C) Putative model of action: DGCR8, under normal post-translational modifications, is able to directly interact with the intronic hairpin of the Tcf7l1 mRNA facilitating the recruitment of the spliceosome. The short Tcf7l1 isoform will allow the differentiation of mESCs (Cavallo et al., 1998; Pereira et al., 2006). When DGCR8 is not present (*Dgcr8*_KO) or hypophosphorylated ($Dgcr8^{mutant}$), it cannot bind to the stem loop structure present in Tcf7l1 mRNA, leading to an inefficient splicing of Tcf7l1. This long Tcf7l1 isoform, enriched in stem cells and down-regulated during differentiation, has been shown to repress lineage specification genes (Wray et al., 2011; Yi et al., 2011). In conclusion, the ratio between the two Tcf7l1 isoforms controls mESCs pluripotency and differentiation.

from an established library (Koike-Yusa et al., 2014). All designs are based on the latest mouse genome assembly (GRCm38/mm10) provided by the University of California, San Cruz, Genome browser (http://genome.ucsc.edu/).

Complementation of mESCs

WT or *Dgcr8*_KO mESCs cells were transfected into six-well plates using Lipofectamine 2000 (Thermo Fisher Scientific) with 2 µg plasmid per well. Cells were plated 24 h before transfection at 200,000 cells per well and cultured in culture medium without streptomycin and penicillin. The medium was changed to normal culture medium 8 h after transfection. After 3 d in the selection media, cells were single sorted into 96-well plates to achieve single-cell colonies. Cells were always cultured in selection media, and positive clones were screened at the DNA, mRNA, or protein level. For DGCR8 complementation, *Dgcr8*_KO–complemented mESCs were achieved by stable transfection of mouse, human, and phosphomutant DGCR8 plasmids (Herbert et al., 2013). Stable independent mESC clones were selected in 250 µg/µl G418-containing medium. For the minigene and short inducible TCF7L1, stable clones were selected in 1 µg/µl puromycin–containing medium.

Plasmids

sgRNAs were individually cloned into the plasmid pX330-U6-Chimeric_BB-CBh-hSpCas9 using the BbsI restriction site as previously described (Cong et al., 2013). The plasmid pX330-U6-Chimeric_BB-CBh-hSpCas9 was a gift from F. Zhang (Massachusetts Institute of Technology, Cambridge, MA; plasmid 42230; Addgene). All of the primers used for the generation of new plasmids are described in Table S2. The human DGCR8 plasmids were a gift from J. Steitz (Yale School of Medicine, New Haven, CT). To generate WT human and phosphomutant DGCR8 constructs under a suitable promoter for stem cell expression, we subcloned the sequence from the original vectors (Herbert et al., 2013) with EcoRI and BglII restriction sites into a pMSCV-neomycin (Takara Bio Inc.). The WT mouse DGCR8 form was amplified by RT-PCR with primers containing the EcoRI and BglII restriction sites. The minigene plasmid was designed with the HiFi DNA Assembly Tool from the New England Biolabs, Inc. website. The exon 4, intronic loop and exon 5 of Tcf7l1 were cloned into the pMSCV-puro vector backbone after digestion with XhoI restriction enzyme. For the easy identification of alternative spliced and WT isoforms, GFP gene-specific primers were added to the external primers (Table S1). For the inducible overexpression of the short Tcf7l1 isoform, the cDNA corresponding to the short Tcf7l1 isoform was cloned from WT mouse differentiated cells into the inducible vector pCW57.1 (plasmid 41393; Addgene) with an infusion cloning kit (Takara Bio Inc.). The expression of the transgene was induced by the addition of 1 µg/ml doxycycline.

Minigene

This construct carries the stem loop present in intron 4 of the *Tcf7l1* gene (840 bp) bound by DGCR8 plus exons 4 and 5 (83 and 133 bp, respectively) cloned into the pMSCV-puro vector backbone. In addition, we added GFP sequences to the 5′ and 3′ ends of the amplified sequence for easy identification. We transiently transfected our Minigene construct in WT mESCs and performed RT-PCR 48 h later with GFP primers (mixed population). Two bands corresponding to the spliced and unspliced isoforms were detected (217 and 1,057 bp, respectively). Next, we transfected our minigene construct and single cloned selected WT and *Dgcr8*_KO mESCs with stable expression under puromycin selection. RT-PCR amplification in WT clones led to a unique band corresponding to the exon 4 and exon 5 spliced form (217 bp). Contrary to this finding, single *Dgcr8*_KO mESCs presented a unique band of 1,057 bp corresponding to the unspliced form.

Genomic DNA extraction and PCR

mESCs were lysed (Tris-HCl 1M, EDTA 0.5M, SDS 20%, NaCl 5M, and ddH_2O) for 4 h at 60°C using proteinase K at 1 mg/ml (Sigma-Aldrich). Genomic DNA was extracted from 1×10^6 mESC pellets using Roti phenol/chloroform/isoamyl alcohol (Roth). Each PCR reaction was performed using 50 ng genomic DNA, and the PCR products were separated on a 1% agarose gel containing ethidium bromide. Genotyping PCR primer sequences are described in Table S1.

Quantitative RT-PCR analysis

Total cellular RNA was extracted from 1×10^6 mESC pellets using TriZOL Reagent (Thermo Fisher Scientific). Extracts quality was verified by loading 1 µg total RNA on a 1% agarose gel. A total of 2 µg cellular RNA was treated with DNase (RQ1 Rnase-Free DNase kit; Promega) and then reverse transcribed according to the manufacturer's protocol using a GoScript Reverse transcription kit (Promega). For each extract, PCR on the *Rrm2* gene was performed, before and after reverse transcription treatment, to ensure the absence of genomic DNA contamination. Quantification of expression levels was performed on a Light Cycler 480 (Roche) using 2 µl of the diluted cDNAs (1:5) and the KAPA SYBR FAST qPCR kit Optimized for Light Cycler 480 (KAPA Biosystems). Differences between samples and controls were calculated based on the $2^{-\Delta CT}$ method. Quantitative RT-PCR assays were performed in triplicate. All the primers needed for the quantitative RT-PCR assays are described in Table S1. For miRNA quantification, 1 µg total RNA was reverse transcribed using the miScript II Reverse Transcription kit (QIAGEN) according to the manufacturer's instructions. After the reverse transcription reactions, cDNA products were diluted five times in distilled water, and 2 µl of the diluted cDNAs was used for PCR using a KAPA SYBR FAST qPCR kit Optimized for Light Cycler 480 (KAPA Biosystems) and miScript Universal Primer (QIAGEN; Table S1). PCR reactions were conducted at 95°C for 10 min, followed by 40 cycles at 95°C for 15 s and 60°C for 30 s on a LightCycler 480 real-time PCR machine (Roche).

Immunoblotting analysis and antibodies

Total cellular protein was extracted from 1×10^6 mESC pellets using a NP-40–based lysis buffer (1% NP-40, 137 mM NaCl, 20 mM Tris-HCl, and 1 mM EDTA) complemented with EDTA-free protease inhibitor cocktail (Roche). Protein concentrations were determined by Bradford Assay (Bio-Rad Laboratories). For each sample, 20 µg total cellular protein was separated in 8% to 10% SDS-PAGE gels and transferred on polyvinylidene fluoride membranes. The following antibodies were used: DGCR8 C-terminal antibody 1:2,000 diluted (10996–1-AP; Proteintech), anti-Oct-3/4 antibody 1:5,000 diluted (611202; BD), Nanog-XP antibody 1:5,000 diluted (D2A3; Cell Signaling Technology), anti-SOX2 antibody 1:10,000 diluted (ab97959; Abcam), anti-DROSHA (D28B1) rabbit mAb (3364; Cell Signaling Technology), TCF-3 antibody 1:1,000 diluted (8635; Santa Cruz Biotechnology, Inc.) was a gift from A. Wutz (ETH Zurich, Zurich, Switzerland), α-tubulin antibody 1:10,000 diluted (A01410; GenScript), rabbit IgG HRP-linked antibody 1:20,000 diluted (08/2012; Cell Signaling Technology), and mouse IgG HRP-linked antibody 1:5,000 diluted (09/2012; Cell Signaling Technology). Immunoblots were developed using the Clarify Western ECL substrate (Bio-Rad Laboratories) kit and detected using an imaging system (ChemiDoc MP; Bio-Rad Laboratories). All membranes were probed with an anti–α-tubulin antibody or Coomassie blue staining to ensure equal loading.

Low-molecular-weight Northern analysis

Total cellular RNA was extracted from 1×10^6 mESC pellets using TriZOL Reagent (Thermo Fisher Scientific). A total of 10 µg total RNA

was resuspended in 30 µl final of 50% deionized formamide, loaded on a 17.5% acrylamide gel (30% acrylamide/bis solution 19:1; Bio-Rad Laboratories), blotted for 1 h on a nylon membrane (Amersham Hybond-NX; GE Healthcare) in 0.5× TBE (Tris/borate/EDTA) buffer at 25 V and 1.5 mA per square centimeter of membrane in a semidry system. Membranes were then ethyl-dimethyl-aminopropylcarbodiimide cross-linked. Prehybridizations and hybridizations were both performed in PerfectHyb Plus Hybridization Buffer (Sigma-Aldrich) at 42°C. All washes were performed in SSC 2×, SDS 0.1%. Radioactive signals were detected with an FLA-7000 device (Fujifilm). For subsequent reprobing, membranes were stripped with boiling 0.1% SDS. miRNA and U6 probes were generated by labeling specific oligonucleotides at the 5′ end using T4 polynucleotide kinase (New England Biolabs, Inc.) and 25 µCi γ[^{32}P]-ATP (3,000 Ci/mmol) and following the manufacturer's instructions. Probes were then purified on Illustra MicroSpin G-25 Columns (GE Healthcare). All of the probes used for miRNA Northern blots are described in Table S1.

DCGR8 RIP

1×10^7 mESCs were washed in 1× cold PBS, scraped, and then lysed with a buffer containing 0.5% Nonidet, 0.5 mM DTT, 20 mM Tris-HCL, pH 7.5, 150 mM KCl, 2 mM EDTA, and inhibitors of RNases, proteases, and phosphatases (Thermo Fisher Scientific). 10% of total lysate was removed and kept as the input samples and the remainder used for immunoprecipitation. 10 µg anti-DGCR8 (Proteintech) or anti-IgG (Sigma-Aldrich) antibody was bound to Sepharose beads (Protein A; Invitrogen) in the presence of heparin. Precleared lysates were then incubated with the appropriate antibody-bound beads, and the immunoprecipitated proteins were then washed (150 mM KCl, 25 mM Tris, pH 7.4, 5 mM EDTA, 0.5 mM DTT, 0.5% NP-40, and RNase, protease, and phosphatase inhibitors) and incubated with DNase I in the presence of DNase buffer (Promega) followed by protease K (New England Biolabs, Inc.) in the presence of 2× protease buffer (New England Biolabs, Inc.). RNA extraction was then performed using phenol-chloroform extraction and ethanol/sodium acetate precipitation. RNA pellets were washed in ethanol, resuspended in 100 µl water, and quantified using a BioPhotometer (Eppendorf).

Exit from pluripotency assay

For the exit from pluripotency assay, 2,000 mESCs were plated in six-well plate at a density of 4,500 cells/cm^2 and then cultured for 3 d in 2i medium (N2B27 +2i +LIF) to adapt the cells to the pluripotent conditions, followed by 4 d of culture in one of two alternative permissive medias (N2B27 without inhibitors or LIF; Figs. 1 D and 2 D; or DMEM + 10% serum; Fig. 4 A) and subsequently for 3 d in 2i medium. The 2i medium was composed of N_2B_{27} (Y40002; Cellartis) complemented with PD032591 at 1 µM final concentration (72184; STEMCELL Technologies), CHIR99021 at 3 µM final concentration (72054; STEMCELL Technologies), 1,000 U/ml of LIF (EMD Millipore), 0.05 mg/ml streptomycin, and 50 U/ml penicillin (Sigma-Aldrich). AP staining was performed using the Alkaline Phosphatase kit (86R-1KT; Sigma-Aldrich) following the manufacturer's instructions. For the quantification of AP positive colonies number, entire six-well plates used for AP staining assays were first scanned to capture the total plate area in a single image. Then, images were processed using the ImageJ software (Nanes, 2015). The number of AP-positive colonies was calculated on threshold intensity (default parameters) of inverted regions that were user-selected (full well or identical areas between conditions) using the Analyze Particles tool (default parameters). The total number of AP-positive colonies is depicted in the graph as a clonal assay.

Proliferation assay

Cells were plated in six-well plates at 75,000 cells per well, and proliferation was assessed every day for 3 d using the CellTiter-Glo Luminescent Cell Viability Assay (G7571; Promega) following the manufacturer's instructions. Proliferation assays were performed in triplicate.

Cell cycle analysis

Asynchronous cells were harvested, washed twice with ice-cold PBS, and fixed in 70% ethanol (a minimum of 24-h incubation at −20°C). Cells were treated with ribonuclease A at 100 µg/ml (R6148; QIAGEN) and incubated in 50 µg/ml propidium iodide for 1 h at 37°C, protected from light. Cells were analyzed by flow cytometry (LSRFortessa; BD) using selective gating to exclude the doublets of cells and subjected to MODFIT analysis (Verity Software House, Inc.). Percentages of cells in G1, S, and G2/M phase were calculated using FLOWJO 7.6.1 software. Cell cycle assays were performed in triplicate.

Flow cytometry analyses

Immunostaining and flow cytometry analyses were performed according to standard procedures. Cells were harvested, washed with PBS, and fixed with 4% paraformaldehyde for 15 min at 37°C. Next, cells were permeabilized for 10 min in 90% methanol on ice. After 1 h at room temperature with the first antibody, secondary antibody was used for 30 min at room temperature. The OCT-4 and NANOG antibodies used are previously listed (immunoblot staining). STELLA antibody (M-150) was purchased from Santa Cruz Biotechnology, Inc. (sc-67249), and anti–human/mouse SSEA-1 eFluor660 antibody was purchased from eBioscience (50-8813-42). Secondary antibodies were purchased from Invitrogen (goat anti–mouse IgG–Alexa Fluor 488 or goat anti–rabbit IgG–Alexa Fluor 546). All antibodies for FACS experiments were used at 1:100 dilutions. Cells were analyzed by flow cytometry (LSRFortessa; BD) using selective gating to exclude the doublets of cells (see legends to Fig. S1, H and I; and Fig. S2 E) and FLOWJO 7.6.1 software. FACS experiments were performed at least three times.

siRNA transfection

mESCs were transfected every 48 h with 60 nM siRNA against long or short Tcf7l1 isoforms (Salomonis et al., 2010) or scrambled control (Mycrosynth) with RNAimax (Invitrogen) following the manufacturer's instructions during the exit of pluripotency and EB differentiation assays (Fig. 4). Verification of Tcf7l1 knockdown was determined by quantitative RT-PCR and immunoblot analysis, as described before.

Statistics

All data are expressed as ±SEM. Statistical differences were measured by Student's *t* test. A value of $P < 0.05$ was considered significant. Data analysis was performed using GraphPad Prism 5.0a software (GraphPad).

RNA-seq

Total cellular RNA was extracted from 1×10^6 mESC pellets using TriZOL Reagent (Thermo Fisher Scientific). The quality of isolated RNA was determined with a Bioanalyzer 2100 (Agilent Technologies) and up to 2 µg poly(A)-purified RNA was used for the library preparation TruSeq Paired-end stranded RNA Preparation kit (Illumina) according to the manufacturer's instructions. Library preparation and sequencing (Illumina HiSeq 2000) were performed at the Functional Genomics Center Zurich. Paired-end sequencing generated ∼2 × 60 million reads per library. Reads from RNA-seq were first preprocessed by trimmomatic (v0.32; Bolger et al., 2014) to remove low-quality ends and adapters. Then, reads were aligned to mouse genome mm10 by STAR (v2.4.2a; Dobin et al., 2013) allowing for at most two mismatches. FeatureCount

(v1.4.5-p1; Liao et al., 2014) was used to count reads for each gene (Ensembl GRCm38.78), ignoring reads on overlapped regions and multiple-hit reads. Differentially expressed genes were defined by both edgeR (v3.12.0; Robinson et al., 2010) and DESeq2 (v1.10.0; Love et al., 2014), with fold change greater than two and false discovery rate <0.1. Differentially spliced events were identified using DEXSeq (v1.16.7) with false discovery rate <0.01 (Anders et al., 2012). A volcano plot was generated using ggplot2 (1.0.1; Ginestet, 2011). Pathway analysis was performed using the Consensus PathDB-mouse database (Kamburov et al., 2013).

Data access

Complete RNA-seq data of WT and *Dgcr8*_KO mESCs are available on the NCBI Gene Expression Omnibus database (GSE78971 for WT mESCs and GSE78974 for *Dgcr8*_KO mESCs).

Online supplemental material

Fig. S1 is a characterization of new CRISPR/Cas9 *Dgcr8*_KO mESCs. Fig. S2 shows that complemented $Dgcr8^{mutant}$ mESCs restored proliferation and cell cycle defects but cannot differentiate. Fig. S3 shows differentially expressed gene pathway analysis, characterization of new CRISPR/Cas9 *Drosha*_KO mESCs, RIP control experiments, and long and short Tcf7l1 differential transcriptional activity experiments and control experiments. Table S1 lists primers. Table S2 lists newly generated plasmids. Table S3 lists differentially expressed genes in *Dgcr8*_KO compared with WT mESCs. Table S4 lists differentially spliced genes in *Dgcr8*_KO compared with WT mESCs.

Acknowledgments

We thank Professor Wutz and Dr. Beyer for critical reading of the manuscript and Dr. Freimann for single-cell sorting. We deeply acknowledge Professor J. Steitz for the DGCR8 plasmids and Professor A. Wutz for gift of the TCF7L1 antibody. Technical help by H. Wischnewski, the Functional Genomics Center Zurich, and the Eidgenössische Technische Hochschule Zürich (ETH) Flow Cytometry Core Facility is gratefully acknowledged.

This work was supported by a core grant from ETH (supported by Roche). D. Cirera-Salinas is supported by the National Centres of Competence in Research RNA and Disease, funded by the Schweizerischer Nationalfonds zur Förderung der Wissenschaftlichen Forschung. M. Bodak is supported by ETH Zurich (ETH-21 13-1) and R.P. Ngondo is supported by Schweizerischer Nationalfonds zur Förderung der Wissenschaftlichen Forschung grant 31003A_153220.

The authors declare no competing financial interests.

Author contributions: D. Cirera-Salinas and C. Ciaudo conceived the study, performed experiments, analyzed data, and wrote the manuscript. M. Bodak and R.P. Ngondo contributed to experiments and data analysis. J. Yu performed the bioinformatics analysis. K.M. Herbert provided critical tools and fruitful discussions.

Submitted: 15 June 2016
Revised: 14 October 2016
Accepted: 12 December 2016

References

Agranat-Tamir, L., N. Shomron, J. Sperling, and R. Sperling. 2014. Interplay between pre-mRNA splicing and microRNA biogenesis within the supraspliceosome. *Nucleic Acids Res.* 42:4640–4651. http://dx.doi.org/10.1093/nar/gkt1413

Ambros, V. 2003. MicroRNA pathways in flies and worms: growth, death, fat, stress, and timing. *Cell.* 113:673–676. http://dx.doi.org/10.1016/S0092-8674(03)00428-8

Anders, S., A. Reyes, and W. Huber. 2012. Detecting differential usage of exons from RNA-seq data. *Genome Res.* 22:2008–2017. http://dx.doi.org/10.1101/gr.133744.111

Bartel, D.P. 2009. MicroRNAs: target recognition and regulatory functions. *Cell.* 136:215–233. http://dx.doi.org/10.1016/j.cell.2009.01.002

Betschinger, J., J. Nichols, S. Dietmann, P.D. Corrin, P.J. Paddison, and A. Smith. 2013. Exit from pluripotency is gated by intracellular redistribution of the bHLH transcription factor Tfe3. *Cell.* 153:335–347. http://dx.doi.org/10.1016/j.cell.2013.03.012

Bolger, A.M., M. Lohse, and B. Usadel. 2014. Trimmomatic: a flexible trimmer for Illumina sequence data. *Bioinformatics.* 30:2114–2120. http://dx.doi.org/10.1093/bioinformatics/btu170

Cavallo, R.A., R.T. Cox, M.M. Moline, J. Roose, G.A. Polevoy, H. Clevers, M. Peifer, and A. Bejsovec. 1998. *Drosophila* Tcf and Groucho interact to repress Wingless signalling activity. *Nature.* 395:604–608. http://dx.doi.org/10.1038/26982

Cirera-Salinas, D., M. Pauta, R.M. Allen, A.G. Salerno, C.M. Ramírez, A. Chamorro-Jorganes, A.C. Wanschel, M.A. Lasuncion, M. Morales-Ruiz, Y. Suarez, et al. 2012. Mir-33 regulates cell proliferation and cell cycle progression. *Cell Cycle.* 11:922–933. http://dx.doi.org/10.4161/cc.11.5.19421

Cole, M.F., S.E. Johnstone, J.J. Newman, M.H. Kagey, and R.A. Young. 2008. Tcf3 is an integral component of the core regulatory circuitry of embryonic stem cells. *Genes Dev.* 22:746–755. http://dx.doi.org/10.1101/gad.1642408

Cong, L., F.A. Ran, D. Cox, S. Lin, R. Barretto, N. Habib, P.D. Hsu, X. Wu, W. Jiang, L.A. Marraffini, and F. Zhang. 2013. Multiplex genome engineering using CRISPR/Cas systems. *Science.* 339:819–823. http://dx.doi.org/10.1126/science.1231143

Dobin, A., C.A. Davis, F. Schlesinger, J. Drenkow, C. Zaleski, S. Jha, P. Batut, M. Chaisson, and T.R. Gingeras. 2013. STAR: ultrafast universal RNA-seq aligner. *Bioinformatics.* 29:15–21. http://dx.doi.org/10.1093/bioinformatics/bts635

Ginestet, C. 2011. ggplot2. Elegant graphics for data analysis. *J.R. Stat. Soc.* 174:245–246. http://dx.doi.org/10.1007/978-0-387-98141-3

Guo, G., Y. Huang, P. Humphreys, X. Wang, and A. Smith. 2011. A PiggyBac-based recessive screening method to identify pluripotency regulators. *PLoS One.* 6:e18189. http://dx.doi.org/10.1371/journal.pone.0018189

Heigwer, F., G. Kerr, and M. Boutros. 2014. E-CRISP: fast CRISPR target site identification. *Nat. Methods.* 11:122–123. http://dx.doi.org/10.1038/nmeth.2812

Herbert, K.M., G. Pimienta, S.J. DeGregorio, A. Alexandrov, and J.A. Steitz. 2013. Phosphorylation of DGCR8 increases its intracellular stability and induces a progrowth miRNA profile. *Cell Reports.* 5:1070–1081. http://dx.doi.org/10.1016/j.celrep.2013.10.017

Herbert, K.M., S.K. Sarkar, M. Mills, H.C. Delgado De la Herran, K.C. Neuman, and J.A. Steitz. 2016. A heterotrimer model of the complete Microprocessor complex revealed by single-molecule subunit counting. *RNA.* 22:175–183. http://dx.doi.org/10.1261/rna.054684.115

Kamburov, A., U. Stelzl, H. Lehrach, and R. Herwig. 2013. The ConsensusPathDB interaction database: 2013 update. *Nucleic Acids Res.* 41(D1):D793–D800. http://dx.doi.org/10.1093/nar/gks1055

Kanellopoulou, C., S.A. Muljo, A.L. Kung, S. Ganesan, R. Drapkin, T. Jenuwein, D.M. Livingston, and K. Rajewsky. 2005. Dicer-deficient mouse embryonic stem cells are defective in differentiation and centromeric silencing. *Genes Dev.* 19:489–501. http://dx.doi.org/10.1101/gad.1248505

Kim, V.N., J. Han, and M.C. Siomi. 2009. Biogenesis of small RNAs in animals. *Nat. Rev. Mol. Cell Biol.* 10:126–139. http://dx.doi.org/10.1038/nrm2632

Koike-Yusa, H., Y. Li, E.-P. Tan, M.C. Velasco-Herrera, and K. Yusa. 2014. Genome-wide recessive genetic screening in mammalian cells with a lentiviral CRISPR-guide RNA library. *Nat. Biotechnol.* 32:267–273. http://dx.doi.org/10.1038/nbt.2800

Leeb, M., S. Dietmann, M. Paramor, H. Niwa, and A. Smith. 2014. Genetic exploration of the exit from self-renewal using haploid embryonic stem cells. *Cell Stem Cell.* 14:385–393. http://dx.doi.org/10.1016/j.stem.2013.12.008

Liao, Y., G.K. Smyth, and W. Shi. 2014. featureCounts: an efficient general purpose program for assigning sequence reads to genomic features. *Bioinformatics.* 30:923–930. http://dx.doi.org/10.1093/bioinformatics/btt656

Loh, K.M., B. Lim, and L.T. Ang. 2015. Ex uno plures: molecular designs for embryonic pluripotency. *Physiol. Rev.* 95:245–295. http://dx.doi.org/10.1152/physrev.00001.2014

Love, M.I., W. Huber, and S. Anders. 2014. Moderated estimation of fold change and dispersion for RNA-seq data with DESeq2. *Genome Biol.* 15:550. http://dx.doi.org/10.1186/s13059-014-0550-8

Macias, S., M. Plass, A. Stajuda, G. Michlewski, E. Eyras, and J.F. Cáceres. 2012. DGCR8 HITS-CLIP reveals novel functions for the Microprocessor. *Nat. Struct. Mol. Biol.* 19:760–766. http://dx.doi.org/10.1038/nsmb.2344

Marks, H., T. Kalkan, R. Menafra, S. Denissov, K. Jones, H. Hofemeister, J. Nichols, A. Kranz, A.F. Stewart, A. Smith, and H.G. Stunnenberg. 2012. The transcriptional and epigenomic foundations of ground state pluripotency. *Cell.* 149:590–604. http://dx.doi.org/10.1016/j.cell.2012.03.026

Marson, A., S.S. Levine, M.F. Cole, G.M. Frampton, T. Brambrink, S. Johnstone, M.G. Guenther, W.K. Johnston, M. Wernig, J. Newman, et al. 2008. Connecting microRNA genes to the core transcriptional regulatory circuitry of embryonic stem cells. *Cell.* 134:521–533. http://dx.doi.org/10.1016/j.cell.2008.07.020

Nanes, B.A. 2015. Slide Set: Reproducible image analysis and batch processing with ImageJ. *Biotechniques.* 59:269–278. http://dx.doi.org/10.2144/000114351

Nguyen, T.A., M.H. Jo, Y.-G. Choi, J. Park, S.C. Kwon, S. Hohng, V.N. Kim, and J.S. Woo. 2015. Functional anatomy of the human microprocessor. *Cell.* 161:1374–1387. http://dx.doi.org/10.1016/j.cell.2015.05.010

Pereira, L., F. Yi, and B.J. Merrill. 2006. Repression of Nanog gene transcription by Tcf3 limits embryonic stem cell self-renewal. *Mol. Cell. Biol.* 26:7479–7491. http://dx.doi.org/10.1128/MCB.00368-06

Robinson, M.D., D.J. McCarthy, and G.K. Smyth. 2010. edgeR: a Bioconductor package for differential expression analysis of digital gene expression data. *Bioinformatics.* 26:139–140. http://dx.doi.org/10.1093/bioinformatics/btp616

Salomonis, N., C.R. Schlieve, L. Pereira, C. Wahlquist, A. Colas, A.C. Zambon, K. Vranizan, M.J. Spindler, A.R. Pico, M.S. Cline, et al. 2010. Alternative splicing regulates mouse embryonic stem cell pluripotency and differentiation. *Proc. Natl. Acad. Sci. USA.* 107:10514–10519. http://dx.doi.org/10.1073/pnas.0912260107

Smibert, P., J.-S. Yang, G. Azzam, J.-L. Liu, and E.C. Lai. 2013. Homeostatic control of Argonaute stability by microRNA availability. *Nat. Struct. Mol. Biol.* 20:789–795. http://dx.doi.org/10.1038/nsmb.2606

Tam, W.-L., C.Y. Lim, J. Han, J. Zhang, Y.-S. Ang, H.-H. Ng, H. Yang, and B. Lim. 2008. T-cell factor 3 regulates embryonic stem cell pluripotency and self-renewal by the transcriptional control of multiple lineage pathways. *Stem Cells.* 26:2019–2031. http://dx.doi.org/10.1634/stemcells.2007-1115

Wada, T., J. Kikuchi, and Y. Furukawa. 2012. Histone deacetylase 1 enhances microRNA processing via deacetylation of DGCR8. *EMBO Rep.* 13:142–149. http://dx.doi.org/10.1038/embor.2011.247

Wang, Y., R. Medvid, C. Melton, R. Jaenisch, and R. Blelloch. 2007. DGCR8 is essential for microRNA biogenesis and silencing of embryonic stem cell self-renewal. *Nat. Genet.* 39:380–385. http://dx.doi.org/10.1038/ng1969

Wang, Y., C. Melton, Y.P. Li, A. Shenoy, X.X. Zhang, D. Subramanyam, and R. Blelloch. 2013. miR-294/miR-302 promotes proliferation, suppresses G1-S restriction point, and inhibits ESC differentiation through separable mechanisms. *Cell Reports.* 4:99–109. http://dx.doi.org/10.1016/j.celrep.2013.05.027

Wettstein, R., and M. Bodak, and C. Ciaudo. 2016. Generation of a knockout mouse embryonic stem cell line using a paired CRISPR/Cas9 genome engineering tool. *Methods Mol. Biol.* 341:321–343. http://dx.doi.org/10.1007/7651_2015_213

Wray, J., T. Kalkan, S. Gomez-Lopez, D. Eckardt, A. Cook, R. Kemler, and A. Smith. 2011. Inhibition of glycogen synthase kinase-3 alleviates Tcf3 repression of the pluripotency network and increases embryonic stem cell resistance to differentiation. *Nat. Cell Biol.* 13:838–845. http://dx.doi.org/10.1038/ncb2267

Yi, F., L. Pereira, and B.J. Merrill. 2008. Tcf3 functions as a steady-state limiter of transcriptional programs of mouse embryonic stem cell self-renewal. *Stem Cells.* 26:1951–1960. http://dx.doi.org/10.1634/stemcells.2008-0229

Yi, F., L. Pereira, J.A. Hoffman, B.R. Shy, C.M. Yuen, D.R. Liu, and B.J. Merrill. 2011. Opposing effects of Tcf3 and Tcf1 control Wnt stimulation of embryonic stem cell self-renewal. *Nat. Cell Biol.* 13:762–770. http://dx.doi.org/10.1038/ncb2283